

Dispersion and Reconstruction

Carolyn R. Mockett

1 Introduction

Since the 1970's physical oceanographers have been using neutrally buoyant floats to make Lagrangian measurements of ocean circulation. Today the use of floats is becoming more and more common, and these measurements are regularly used to make maps of the Eulerian flow. Yet the relationship between Eulerian and Lagrangian statistics has been not been fully explored. One can approach this relationship from two directions. The first is given a certain Eulerian flow field, what can one say about the Lagrangian float trajectories? The inverse of this is given the Lagrangian float trajectories what can one say about the Eulerian flow?

There has been work on the dispersion of passive particles in 2-D turbulence. But there has not been a full exploration of the effects of β and the free surface on dispersion, both of which are factors in large scale flow in the ocean. In addition what are the direct and indirect effects of vortices on dispersion with β and a free surface? An improved understanding of dispersion in different types of flow will assist in better understanding float data.

The inverse question of starting from the Lagrangian data and attempting to reconstruct the Eulerian field is a broad topic. A simple place to start is to add a zonal flow to a turbulent background and test various factors that effect how well one succeeds in recovering the mean from Lagrangian measurements.

2 The Model

To explore both of these questions a series of numerical experiments have been carried out that integrated the equivalent barotropic quasigeostrophic equation in dimensionless form. It is given by:

$$\frac{\partial q}{\partial t} + [\psi, q] + \beta \frac{\partial \psi}{\partial x} = -\mu \nabla^6 \psi$$

The vorticity q is given by $q = \nabla^2 \psi - F\psi$, where $\nabla^2 \psi$ is the relative vorticity and $F\psi$ is the free surface term. $F = (L/L_R)^2$ where L is the length scale of the domain and $L_R = \frac{(g'H)^{\frac{1}{2}}}{f}$ is the Rossby radius of deformation. The Rossby radius gives a length scale at which the effects of rotation become important. There is no forcing so the field is freely decaying, and a hyper viscosity is used with $\mu = 5 \times 10^{-7}$.

The numerical integration is done on a doubly periodic square lattice $(0, 2\pi; 0, 2\pi)$ with 128x128 resolution. The code is pseudo-spectral with standard 2/3 dealiasing. Pseudo-spectral

means that the derivatives are done in spectral space while the the products are done in physical space. A 3rd order Adams-Bashforth scheme is used for the time-integration.

To calculate the float trajectories one needs to integrate $\dot{x} = -\frac{\partial\psi}{\partial y}$, $\dot{y} = \frac{\partial\psi}{\partial x}$. Again 3rd order Adams-Bashforth scheme is used for the time integration and the spatial interpolation of position between grid points is done with cubic spectral splines.

All the runs are started with a random Gaussian vorticity field with narrow band wave number spectrum. The initial kinetic energy spectrum is given by $E(k) = \frac{E_o k^6}{(2k_o+k)^{18}}$, where $k_o = 15$, and E_o is fixed such that the total energy $E = \int E(k)dk = 0.5$. The initial field then freely evolves. As energy cascades to larger scales vortices form. They interact, and merge, and with time there are fewer and fewer vortices since there is no forcing. Since these flows are freely decaying one must worry about their stationarity. The hope is that the flow is sufficiently stationary over the time period analyzed, during which the total energy only decreases by about 2%. One can also argue that there is no reason to believe the ocean itself is stationary.

After the vortex formation period, a 32x32 uniform grid of floats are put in the flow and passively advected. Each float measures position (x, y) , velocity (u, v) , the stream function ψ , and vorticity $\nabla^2\psi - F\psi$ every $dt = .1$, from $t = 0$ to $t = 40$. Since there are periodic boundaries, the trajectories are unfolded before calculating dispersion statistics. Therefore the final area of the unfolded float trajectories can be much larger than the original 128x128 domain. The Eulerian velocity field is recorded on the same uniform grid where the floats were initially seeded. In order to have the same amount of data in the Eulerian data set as the Lagrangian, the Eulerian velocities are also recorded every $dt = .1$ for the same length of time.

The dimensional and non-dimensional scales this model corresponds to are $U \sim .2m/s$, $U^n \sim .6$, $L \sim 400km$, $L^n = 2\pi$, $L_\beta \sim 150km$, $L_\beta^n \sim 2$, $L_R \sim 70km$, $L_R^n \sim 1$, and $T \sim 3days$, $T^n = 1$. A superscript n refers to non-dimensional. The Rhines scale, $L_\beta = \sqrt{\frac{U}{\beta}}$ gives an (upper) estimate of the scale at which Rossby waves dominate over vortices.

3 Part I: Dispersion

3.1 Definitions

In order to explore the dispersion of floats there are certain statistics that are useful. To begin with absolute dispersion measures the mean square displacement of an ensemble of floats at a given time. It is defined as

$$A(t)^2 = \langle (x(t) - x(0))^2 \rangle$$

where $\langle \dots \rangle$ is an average over an ensemble of floats and $x(0)$ is the initial position of a float. One can also define the dispersion coefficient by

$$D(t) = \frac{A^2}{2t}$$

Taylor(1921) obtained two limits for $D(t)$ in isotropic, homogeneous, stationary turbulence

$$D \propto t \quad \text{when } t \rightarrow 0$$

$$D = \text{Const.} \quad \text{when } t \rightarrow \infty$$

This first limit is called ballistic diffusion, while the second is Brownian diffusion. Single particle diffusion is a good measure of the mean displacement of floats. But if one wants to know more specifically how floats are dispersing, it is useful to define a PDF of displacement. This is given by

$$p(d) = \frac{n(d)}{N\Delta d}$$

where $n(d)$ is the number of floats that have been displaced a distance between d and Δd , N is the total number of floats, and Δd is the width of the bin.

Another useful tool is the power spectrum. Given

$$S(\nu) = \int_0^T u'(t) e^{-i2\pi\nu t} dt$$

where $u'(t) = u(t) - \overline{u(t)}$ is for a given float or Eulerian velocity time series, and $\overline{u(t)}$ is the mean of that time series. ν is the frequency. The power spectrum $P(\nu)$ is given by:

$$P(\nu) = \frac{1}{T} [S(\nu) \cdot S^*(\nu)]$$

The spectrum was calculated for each float and then averaged over all floats. The same was done with the Eulerian data.

As a word of caution, note that all the previously defined statistics have been developed for statistically stationary processes. Since our turbulence is decaying, strictly speaking we are out of the domain of applicability of the methods and their use must be considered heuristic. However, the energy decay is very slow and as a good approximation the dynamics may be considered stationary.

Previously it has been demonstrated that the form of dispersion for passive particles in vortices is different from those in the background (Elhmaidi et al. 1993). To distinguish between these two regions one can use the Okubo-Weiss parameter $Q(x, y, t) = S^2 - \omega^2$, where S^2 is the sum of the squares of the normal and shear components of strain, and ω is the vorticity. The only problem is that strain and vorticity are very difficult to measure in the ocean with floats. Rupolo et al (1996) used low and high kinetic energy (KE) as a proxy to distinguish between floats in and out of vortices. Since the goal of this project is to explore dispersion of floats, high and low KE will be used to make this distinction. The 200 floats with the highest kinetic energy and with the lowest kinetic energy will be used for the high KE floats, and the low KE floats respectively.

3.2 The Four Cases Considered

To examine the effects of β and a free surface on dispersion the natural thing to do is look at four different cases: Case 1 ($\beta = 0, F = 0$), Case 2 ($\beta = 5, F = 0$), Case 3 ($\beta = 0, F = 30$), Case 4 ($\beta = 5, F = 30$). In order to start each case with the same kinetic energy $F\psi$ was subtracted from the initial relative vorticity field used to start Cases 1 and 2 to obtain a new vorticity field to start Cases 3 and 4. However, since the fields evolved differently Cases 3 and 4 have half the kinetic energy of Cases 1 and 2. Therefore one cannot compare the magnitude of the absolute dispersion between these two pairs, but one can compare the form of the dispersion.

3.2.1 Case 1: $\beta = 0, F = 0$

With $F = 0$ there is no physical limit on the size of the vortices and there are long spatial correlations. This makes it a difficult case to study since quickly the vortices grow and form large scale flow (Figure 1 b) which can bias the dispersion. Regardless of these difficulties this case presented the main features of the dispersion as one would expect. There are comparable displacements in x and y as is evident from the dispersion coefficients (Figure 2 c). Also from the plot of the dispersion coefficient one can see that there is ballistic dispersion at small t , while relatively Brownian dispersion at large times. From the spectrum (Figure 3 a,b) one can see that there is more energy in high frequencies ($\nu \approx 1$) in the Lagrangian data than in the Eulerian data. This reflects that floats travel more rapidly through different parts of the flow than the rate at which the flow changes at a given point and the general process of formation of small space and time scales in advected tracers even for smooth Eulerian flows. When the floats are divided into high KE and low, the high KE floats have much more energy at high frequencies than the low KE floats. This is due to the fact the high KE floats are in the vortices. In addition there is a $-1/4$ slope to the high KE floats previously observed for high KE floats in the ocean (Rupolo et al. 96), which is a possible sign of anomalous diffusion (diffusion that is not Brownian).

3.2.2 Case 2: $\beta = 5, F = 0$

The first thing that is evident when one looks at the contours of vorticity of this case (Figure 1 c,d) is the lack of vortices. The presence of β allows Rossby waves, which have been shown to alter both the dispersion directly and through their inhibition of the formation of vortices (McWilliams 84). If β is large enough Rossby waves can eliminate vortices. The Rhines scale gets smaller as β increases, so the spatial scale over which Rossby waves dominate decreases. This case clearly is dominated by Rossby waves. From Figure 4 a,b one can see that there is much greater x -displacement than in Case 1 because of the waves. There also is a greatly repressed y -displacement since now for a float to move north or south it must cross contours of planetary vorticity. In order to conserve potential vorticity a north-south displacement requires a change in the free surface or relative vorticity to balance the change in planetary vorticity. From (Figure 4 c) one can see from the plot of the dispersion coefficient a long ballistic period until almost $t=1$.

To compare Eulerian statistics to Lagrangian, the energy spectrum (Figure 5 a,b) provides a good comparison. The strong peaks from the waves which are clearly visible in the Eulerian spectrum are absent in the Lagrangian. Since the floats travel with the waves they do not detect them.

It should also be noted that because there are no vortices there is little difference between high and low kinetic energy floats as seen in their spectrum (Figure 5 c,d). In this case, the only difference is that the low KE floats display some indication of the Rossby wave peaks. Thus statistics for high and low KE floats appear to differ significantly only in the presence of vortices.

3.2.3 Case 3: $\beta = 0, F = 30$

With the addition of the free surface the inverse cascade of energy to scales larger than L_R is slowed down. In addition interaction between vortices at distances larger than L_R is shielded, and the dynamics become more localized. This can be seen in Figure 1 e,f. The vortices are $O(L_R)$ so their movement is very slow. The slowness of the vortex movement is most evident when looking at the trajectories of the high and low KE floats (Figure 7 a,b). The high KE floats are trapped in vortices and confined to small areas, while the low KE floats are dispersing through this field of almost stationary vortices. As a consequence the x and y displacement (Figure 7 c) of the high KE floats is repressed by about 1/2 compared to the mean of all floats, and almost all of the energy is at high frequencies (Figure 8 c). For low KE floats there is a greater x, y -displacement (Figure 7 d) than the mean. On the plot of the dispersion coefficient (Figure 7 f) one also notes that there is a longer ballistic dispersion until almost $t = 1$.

For this case the Eulerian and float spectrum (Figure 8 a,b) are especially different. In fact the Eulerian spectrum has not yet leveled off. This is due to the slow motion of the vortices. For the Eulerian time series one vortex can come by and skew the mean such that the time series with the mean removed has long sections of essentially constant velocity and one or a few large jumps. As a consequence the Eulerian spectrum does not level off. With enough time several vortices would come by and the mean would begin to make sense. For this reason the memory in the Eulerian flow is especially long.

3.2.4 Case 4: $\beta = 5, F = 30$

This final case is the most interesting since it combines both the effects of β and the free surface, and is the most applicable to actual ocean dynamics. For this case the x -displacement (Figure 9 a) is twice as large as Case 3 ($\beta = 0, F = 30$). There also is an interesting skew PDF of x -displacement (Figure 9 c). The cause of this becomes very clear when the high KE floats are examined separately. The y -displacement (Figure 9 b) on the other hand is 2/3 less than Case 3 since now β is present. But interestingly the y -displacement is almost twice that of Case 2 ($\beta = 5, F = 0$) even though Case 2 has more kinetic energy. Therefore one can conclude that vortices must contribute to y dispersion.

For the high KE floats there is a smaller x -displacement by 2/3 than the mean, and large net westward displacement (Figure 10 c). The vortices are clearly traveling westward and are

responsible for this behavior. This can also be seen in the PDF of x -displacement which has westward migration with time (Figure 10 e). The low KE floats on the other hand have a comparable x -displacement to the mean and a slight net Eastward displacement (Figure 10 c). There is also noticeably longer ballistic period. Both have similar y displacements.

3.3 Conclusions of Part I

There are large differences between Eulerian and Lagrangian statistics. In particular there is a much longer memory in the Eulerian field, as indicated by the large power in the low-frequency components of the spectrum, which is a reflection of the different characteristics of each method of measurement. By comparing Case 2 with the other three one can also see that coherent structures alter the overall dispersion. Not only do they alter the dispersion but there are different dispersion properties for floats in vortices and those in the background in all three cases with vortices. In particular vortices decrease the ballistic period. This was seen by Elhmaidi et al. 1993 in two dimensional turbulence (Case 1) but it also evident with β and F . Separating the floats into those in and out of vortices allows one to see which are dispersing more. By comparing the displacement of low KE floats to high KE it appears that vortices contribute to dispersion by the flow they set up, but it is not the particles in the vortices (high KE) that disperse the most. It is the particles outside them (low KE) that do. This is evident from Case 3 and Case 4. For these turbulent flows high and low KE is a good proxy for distinguishing between floats that are in or out of vortices.

Finally the addition of β alters the dispersion. It greatly represses dispersion in y , and causes vortices to travel westward as well as the particles they have trapped. Vortices do assist in over coming the effects of β since there is more y dispersion in Case 4 than Case 2, even though Case 2 has more kinetic energy. The Rhines scale also plays an important role in dispersion on the β -plane. Dispersion in the x becomes almost ballistic again after a displacement near the Rhines scale, while y dispersion is essentially halted.

4 PART II: Reconstructing the Mean Flow

The second half of this research approaches the relationship between Eulerian and Lagrangian measurements from the other direction. What factors contribute to how well one can reconstruct the mean Eulerian flow from float data? Although there are numerous things one could test, one can begin with the spatial resolution of initial position of the floats, how often each float measures the flow, and the ratio of the kinetic energy of the mean flow to the kinetic energy of the eddies $KE_{ratio} = KE_{Jet} / KE_{Eddy}$. One can also explore the error that is induced by how the velocity is determined, whether it is directly measured or inferred from float trajectories as is done with ALACE floats (Davis et al., 96).

In order to add a mean flow, a simple sinusoidal vorticity field is added to the initial vorticity field of Case 4 ($\beta = 5, F = 30$). The resulting velocity field is a jet in the center of the domain traveling eastward and westward flow along the top and bottom of the domain. The jet and the turbulent background are then allowed to freely evolve together before the floats are added. The resulting mean zonal velocity is no longer a sinusoid. The jet has extracted

some of the kinetic energy from the eddy field. Figure 11 shows example stream lines for two different strength jets. The first set of stream lines (a,b) is the most energetic case examined, KE ratio=1.4. The vortices are confined to the regions of minimum velocity. One can see from the second set (c,d) when the KE ratio=.312 there are is a much more substantial spatial and temporal variability in jet. The KE of the jet is determined from the mean Eulerian flow $\frac{1}{2}\overline{u_e^2}$, where $\overline{u_e^2}$ is averaged over all the Eulerian data. The eddy KE is found by subtracting this estimate of the KE of the jet from the total KE of the domain, $KE_{Eddy} = KE_{Total} - KE_{Jet}$.

4.1 Perfect Data

With the numerical model the floats act as perfect roving current meters measuring the exact Eulerian velocity at varying locations over time as they follow a fluid parcel. So the comparison between Eulerian data and Lagrangian is purely an issue of resolution (temporally and spatially) since both are making exact measurements. Both Eulerian and Lagrangian velocity measurements are binned in 128x8 rectangles to reconstruct the mean flow averaged over x. All the unfolded trajectories outside the initial 128x128 domain are discarded. Floats are not allowed to wrap around and continue to measure the field. This was done to emphasize one of the drawbacks of floats, that they can leave the area of interest.

Figure 12 shows two reconstructions for two different strength jets. The floats reconstruct the flow quite well, even with as few as 16 floats. But in the less energetic jet there appears to be a systematic underestimate of the peaks of the jet regardless of the number of jets. This is evident in all of the runs at the lower energies.

4.2 Imperfect Data

Since the “perfect” data works very well, we now explore what happens when the velocity is inferred from the float position data. There is a type of float used by oceanographers that are ballasted to sink to certain depth and travel with the flow untracked on the order of weeks, after which they surface and relay their location to a satellite, and then submerge again. The velocity is inferred from the where the float went down and where it next resurfaces and the time in between.

To mimic this type of flow measurements one can reconstructed u and v from trajectories in a similar manner using a centered difference scheme:

$$u(x_i) = \frac{x_{(i+1)} - x_{(i-1)}}{2\Delta t}$$

$$v(y_i) = \frac{y_{(i+1)} - y_{(i-1)}}{2\Delta t}$$

$\Delta t = .1, .4, 1, 2$ were used. The data is thinned temporally, such that $x_{(i+1)}$ and $x_{(i-1)}$ are $2\Delta t$ apart. A $\Delta t = 1$ is between once and twice an eddy turn over time depending on the strength of the mean flow. Measurements are then analyzed the same way as the “perfect” data.

To approximate the two-week period the ALACE floats are submerged, a $\Delta t = 2$ is used since a non-dimensional time unit is about three days and a centered difference has a time

separation of $2\Delta t$. In Figure 13 one can see that the underestimate of the peaks of the jet is now significant. To ensure this was not due to the lack of data, there also is a plot of the “perfect” data thinned temporally by $\Delta t = 2$ to compare it to. The thinned “perfect” data actually slightly over estimates the peaks. Therefore one can conclude that this method of reconstructing the mean velocity is introducing some type of systematic error.

4.3 Energy of mean flow vs. energy of eddies

To explore whether the ratio of the kinetic energy of the mean flow to the kinetic energy of the eddies is a key factor, several runs were done with the magnitude of KE ratio varying from 1.4 to .18 . The rms error between the the Lagrangian velocity and Eulerian divided by the total rms velocity of the Eulerian mean is then plotted as a function of the KE ratio. This was calculated with all 1024 floats, 256 floats, 64 floats, and 16 floats.

For the most energetic jet there is an increase in error since the floats move quickly through the domain and there are less measurements, but as the KE ratio of the flow decreases below .7 the error begins to increase again and reaches forty percent. One will also note that with the “perfect” data (Figure 14 a)the number of floats does not seem to matter much, all the error curves lie close together.

The same procedure is applied to the reconstructed velocities. For $\Delta t = .1$ (Figure 14 b)the plot looks similar to the “perfect” data, but now there is a spreading of the error lines of different number of floats. For $\Delta t = 1$ (Figure 14 d) the whole curve flattens out and the error from the way the velocity field was reconstructed masks the error determined by the KE ratio .

4.4 Conclusions of Part II

Overall there is an underestimate of the jet strength when using float data especially as the KE ratio decreases. As the KE ratio decreases it becomes much more difficult to detect the mean and the error can rise to forty percent. The underestimate is particularly evident when the velocities are reconstructed from the trajectories using a centered difference. The longer Δt one uses to reconstruct the velocity field, the larger the underestimate. In addition the number of floats becomes much more important when the velocity is reconstructed from trajectories since each measurement contains a certain level of error. In fact if the data is “perfect” one can do basically as well with only 16 floats as 1024 floats.

5 Future Work

For the study of dispersion:

To improve the stationarity of the statistics all four cases should be re-run at higher resolution (512x512), so the friction can be decreased. This will cause less decay of the total energy and potential vorticity. One can also do runs that explore relative dispersion in all four cases by seeding pairs of floats close together. This is something that is being done with floats in the ocean now. It would be interesting to compare the numerical data set with a real one.

For the exploration of flow reconstruction from Lagrangian data:

Since reconstructing the velocities from float trajectories causes a systematic underestimate of the jet peaks the next thing to look at would be the effects of other imperfections in float measurements, like drift, finite size of a float, etc... One could also look at how well Lagrangian float measurements compare to the Eulerian ones with a north-south mean flow, and more complicated mean flows.

Acknowledgements

This work was done with Antonello Provenzale. I also would like to thank Steve Meacham and Eric Chassignet for useful discussions and their enthusiasm for the project.

References

- [Bartello and Holloway, 1991] Bartello, P. and Holloway, G. (1991). Passive scalar transport in β -plane turbulence. *J. Fluid Mech.*, 223:521–536.
- [Davis, 1996] Davis, R. (1996). Comparison of autonomous lagrangian circulation explorer and fine resolution antarctic model results in the south atlantic. *J. Geophys. Res.*, 101(C1):855–884.
- [Elhmaildi et al., 1993] Elhmaildi, D., Provenzale, A., and Babiano, A. (1993). Elementary topology of two-dimensional turbulence from a lagrangian viewpoint and single-particle dispersion. *J. Fluid Mech.*, 257:533–558.
- [Maltrud and Vallis, 1991] Maltrud, M. and Vallis, G. (1991). Energy spectra and coherent structures in forced two-dimensional and beta-plane turbulence. *J. Fluid Mech.*, 228:321–342.
- [McWilliams, 1984] McWilliams, J. (1984). The emergence of isolated coherent vortices in turbulent flow. *J. Fluid Mech.*, 146:21–43.
- [Owens, 1991] Owens, W. (1991). A statistical description of the mean circulation and eddy variability in the northwestern atlantic using sofar floats. *Prog. Oceanog.*, 28:257–303.
- [Provenzale, 1998] Provenzale, A. (1998). Transport by coherent barotropic vortices. *Annual Review*. in press.
- [Rupolo et al., 1996] Rupolo, V., Hua, B., Provenzale, A., and Vincenzo, A. (1996). Lagrangian velocity spectra at 700 m in the western north atlantic. *Physical Oceanography*, 26(8):1591–1606.
- [Taylor, 1921] Taylor, G. (1921). Diffusion by continuous movement. *Proc. Lond. Math Soc.*, 20:196–212.
- [Wiess et al., 1997] Wiess, J., Provenzale, A., and McWilliams, J. (1997). Lagrangian dynamics in high-dimensional point-vortex system. *Physics of Fluids*. submitted.

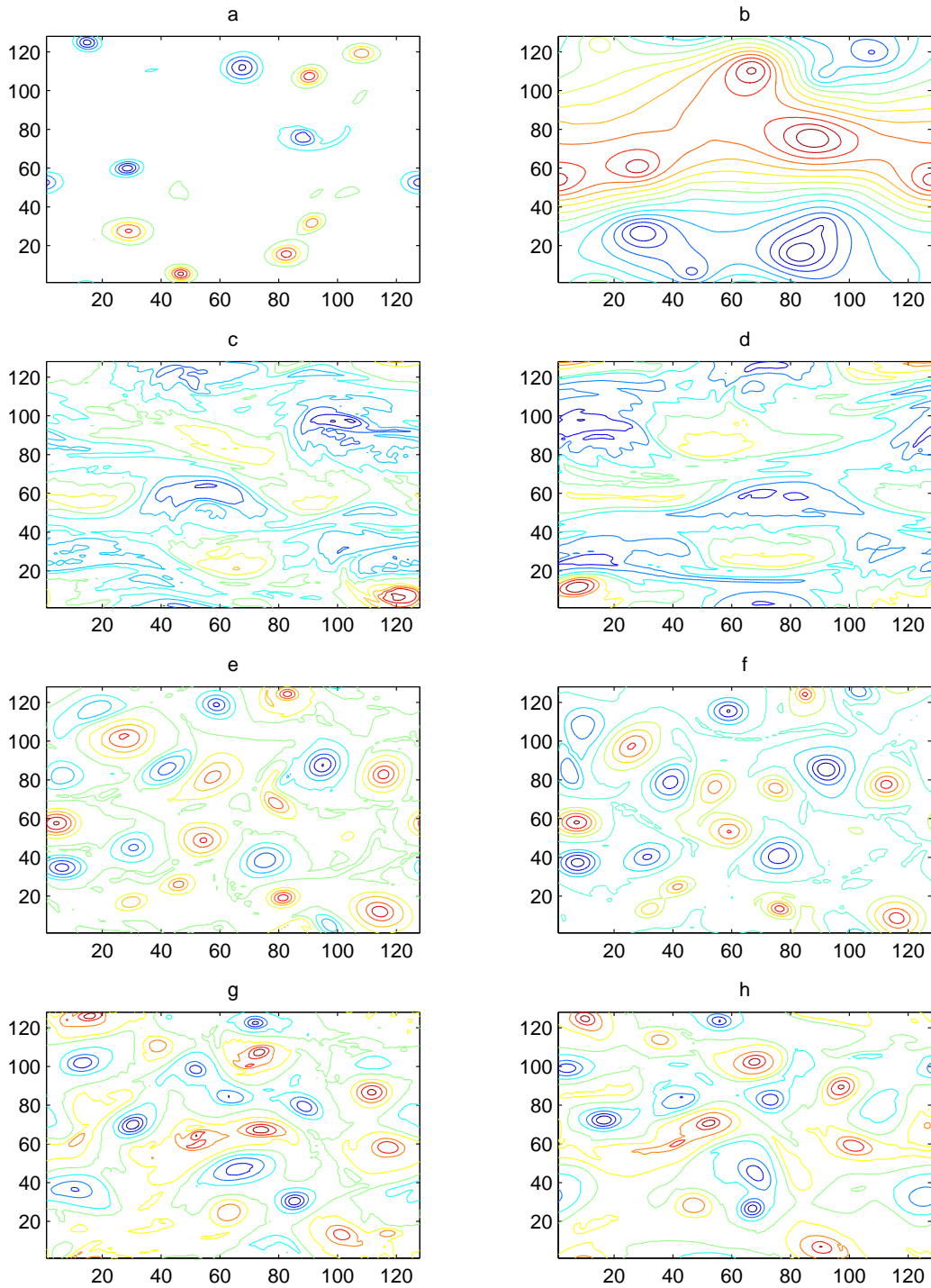


Figure 1: a) CASE 1 contours of vorticity at $t=15$, b) CASE 1 contours of ψ at $t=15$, c,d) CASE 2 contours of vorticity at $t=15,20$, e,f) CASE 3 contours of vorticity at $t=15,20$ g,h) CASE 4 contours of vorticity at $t=15,20$.

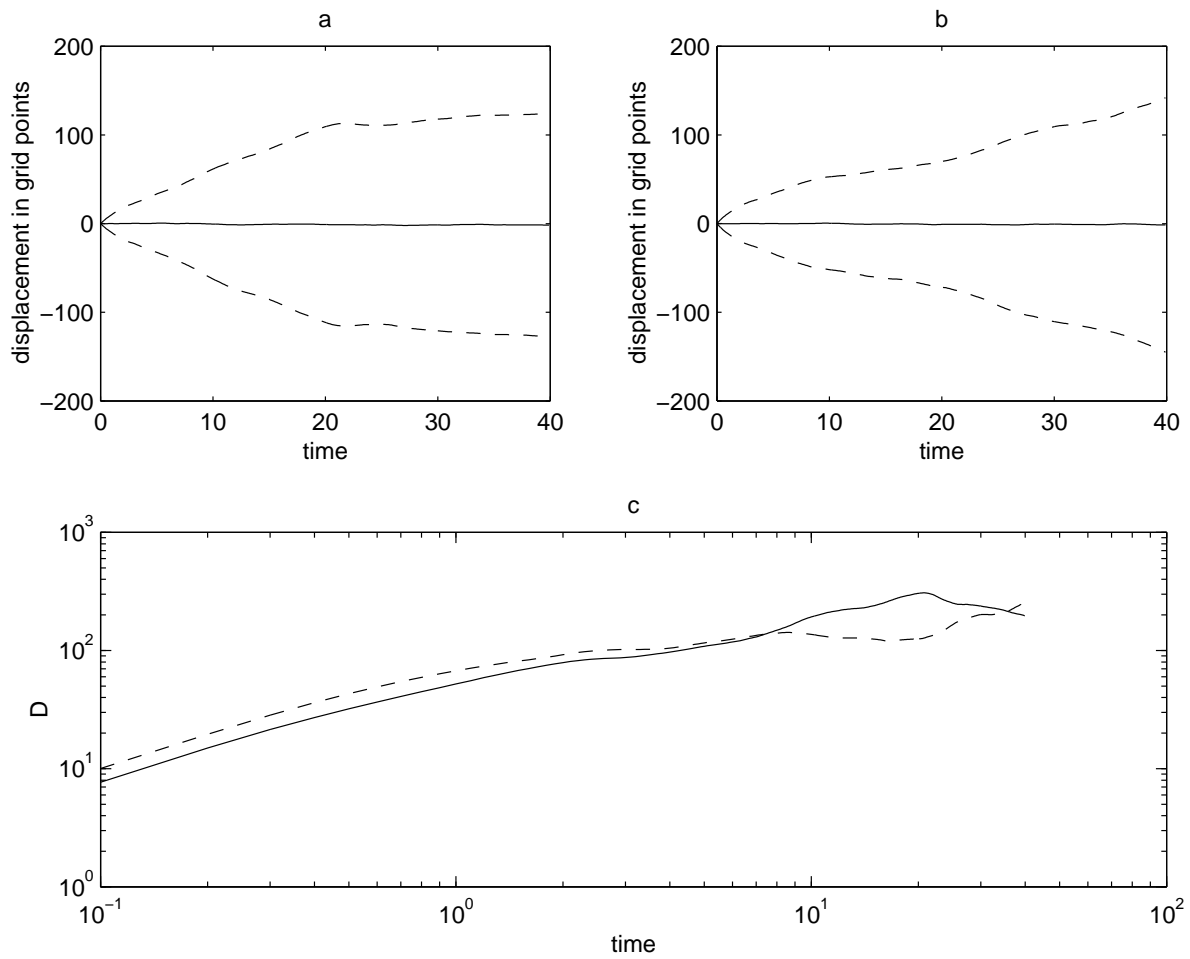


Figure 2: CASE 1 a) the solid line is the mean x-displacement, and the dashed are plus and minus A, the rms. b) the solid line is the mean y-displacement, and the dashed are plus and minus A, the rms. c) The dispersion coefficient, solid line -in x, dashed line - in y.

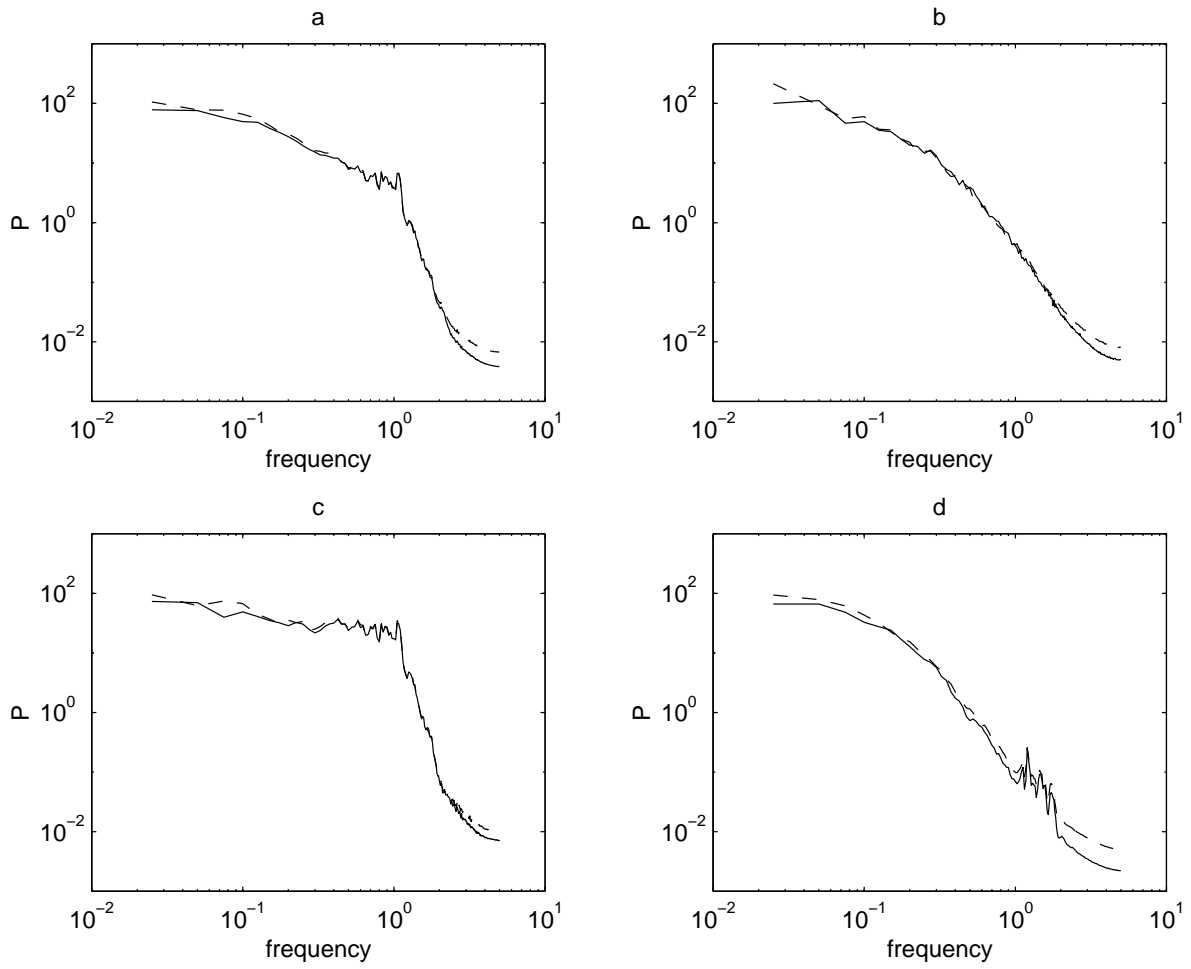


Figure 3: CASE 1 The power spectrum from u(solid), v(dashed). a) the floats. b)the Eulerian field. c) high KE floats. d) low KE floats

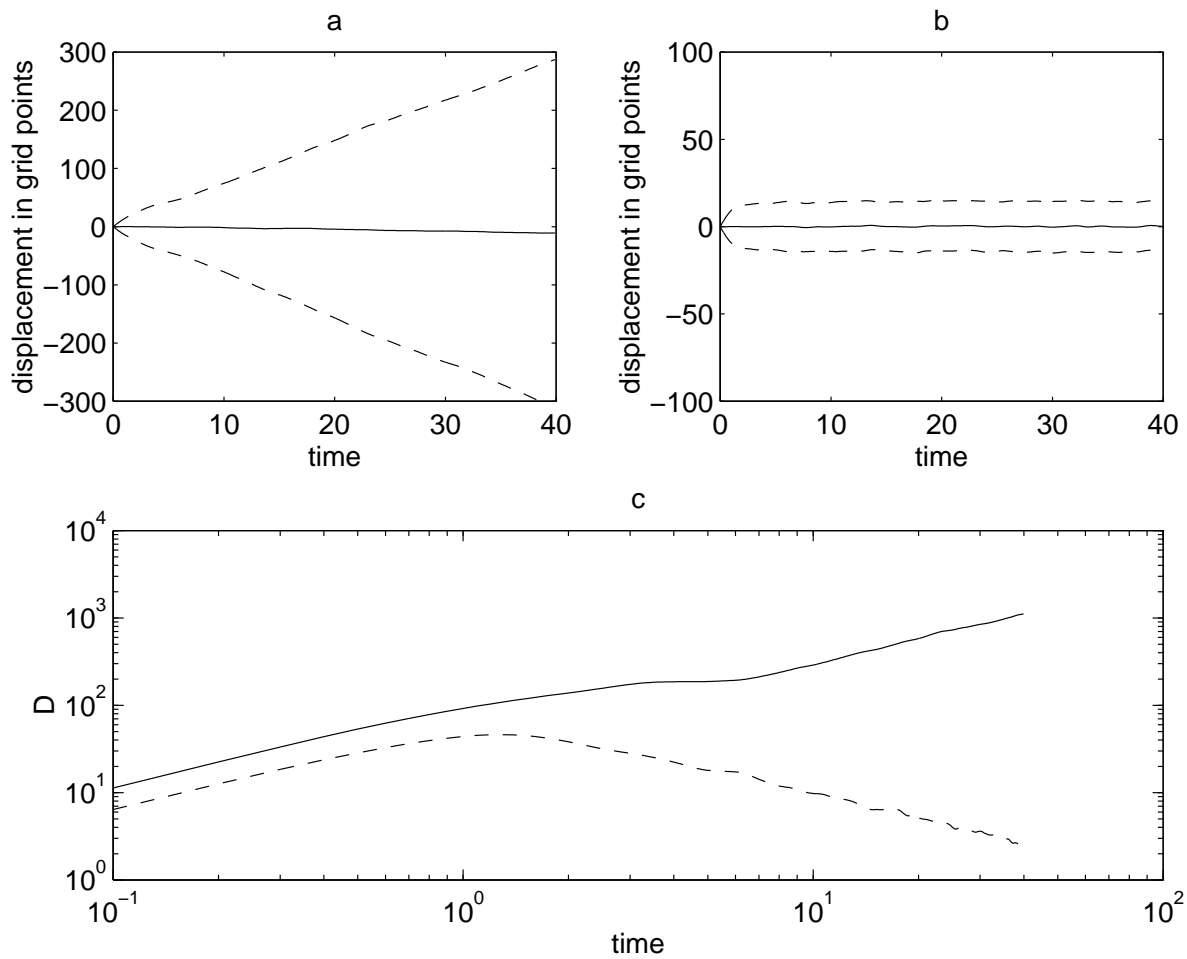


Figure 4: CASE 2 a) the solid line is the mean x-displacement, and the dashed are plus and minus A , the rms. b) the solid line is the mean y-displacement, and the dashed are plus and minus A , the rms. c) The dispersion coefficient, solid line - in x, dashed line - in y.

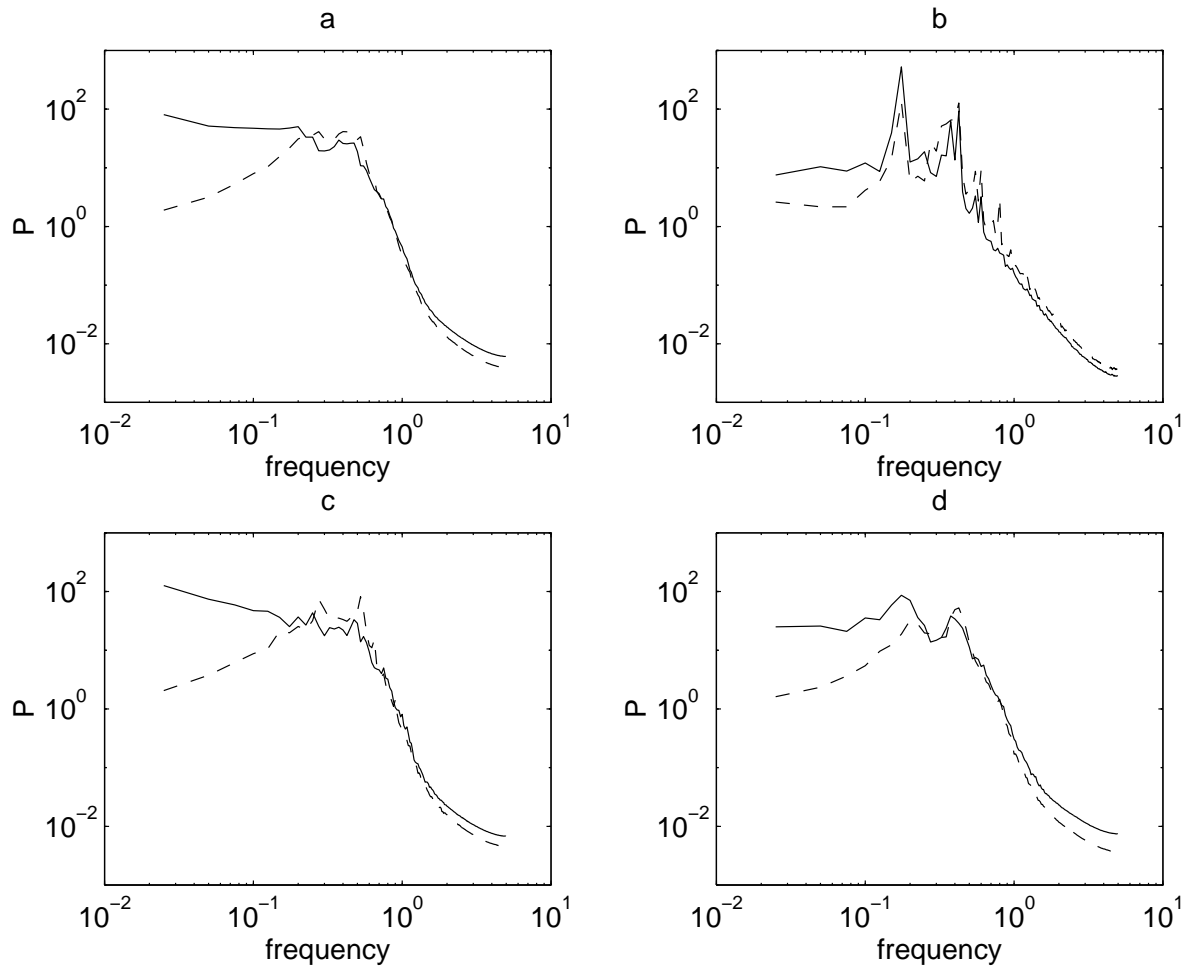


Figure 5: CASE 2 The power spectrum from u (solid), v (dashed). a) the floats. b)the Eulerian field. c) high KE floats. d) low KE floats

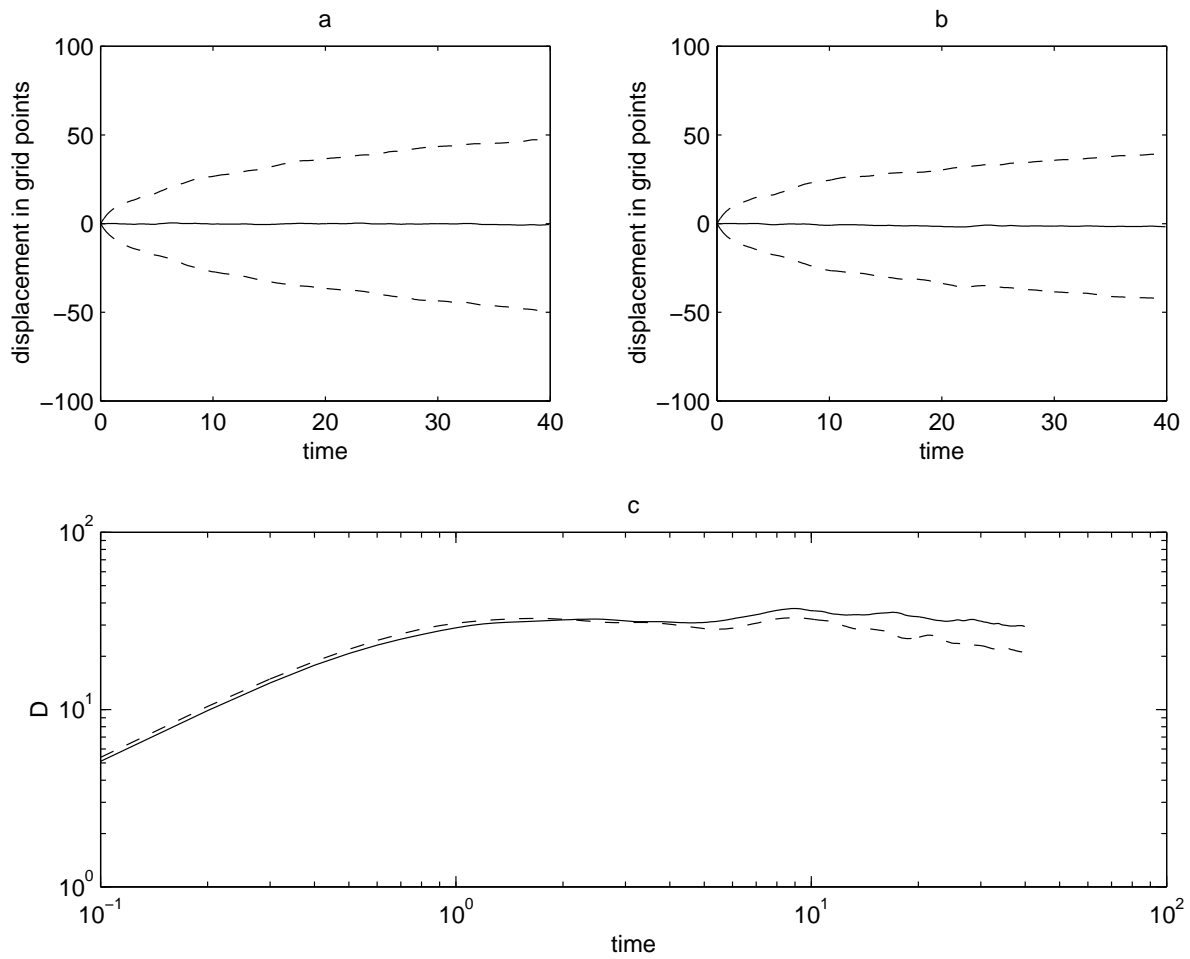


Figure 6: CASE 3 a) the solid line is the mean x-displacement, and the dashed are plus and minus A , the rms. b) the solid line is the mean y-displacement, and the dashed are plus and minus A , the rms. c) The dispersion coefficient, solid line - in x, dashed line - in y.

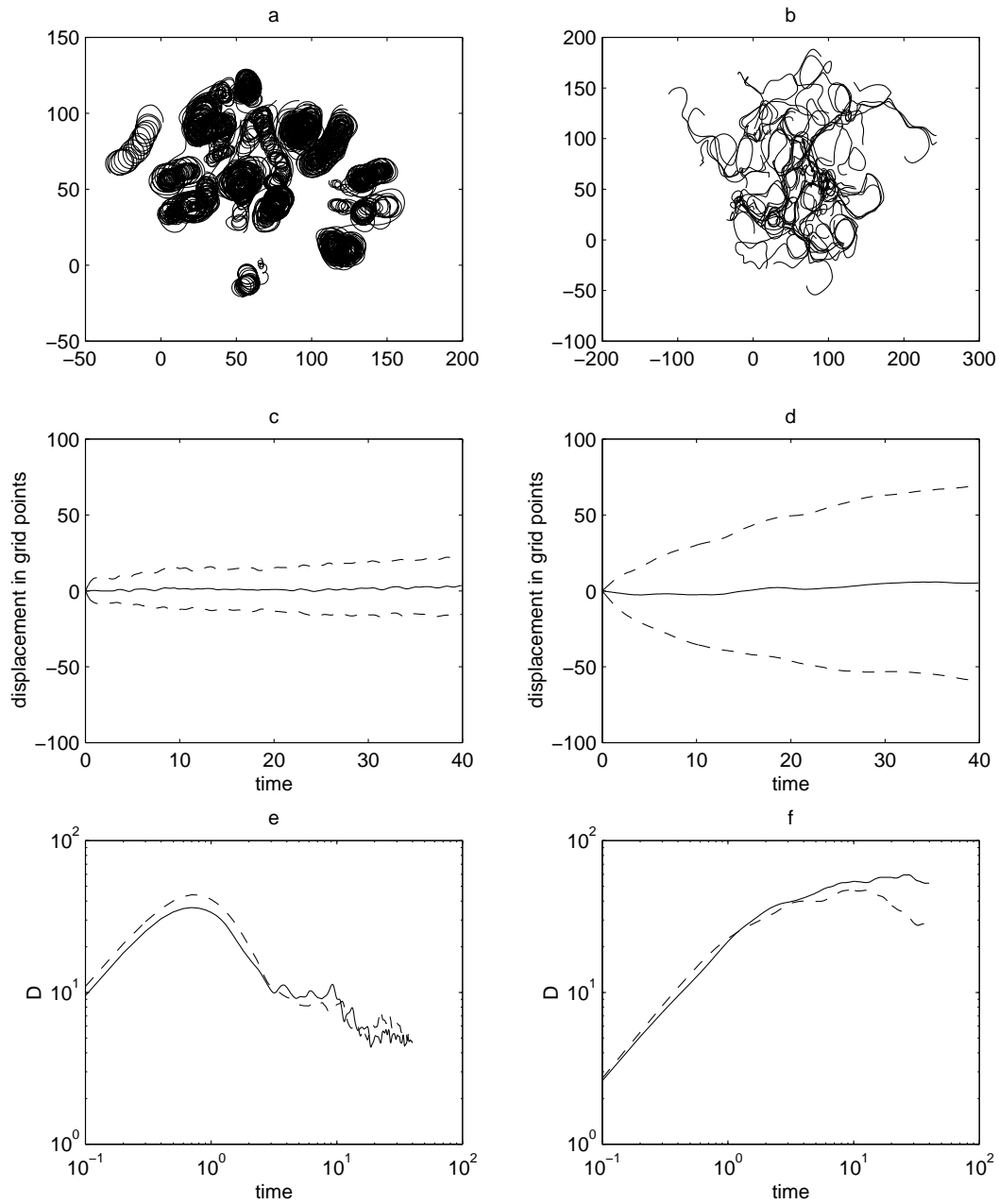


Figure 7: CASE 3 a) The trajectories of high KE floats, b) The trajectories of low KE floats, c) high KE floats: the solid line is the mean x-displacement, and the dashed are plus and minus A , the rms. d) low KE floats: the solid line is the mean x-displacement, and the dashed are plus and minus A , the rms. e) The dispersion coefficient for the high KE floats, solid line -in x, dashed line - in y. f) The dispersion coefficient for low KE floats, solid line -in x, dashed line -in y.

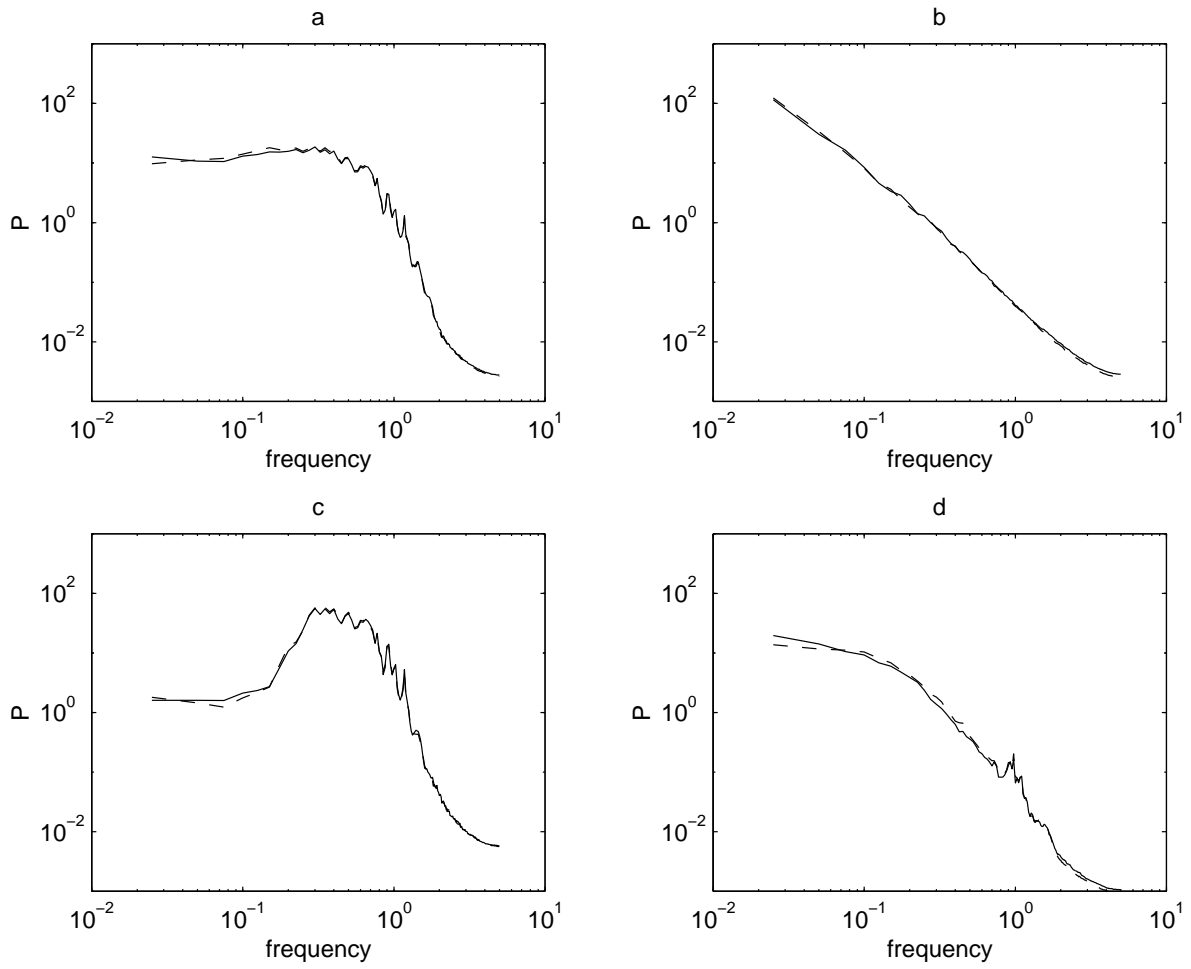


Figure 8: CASE 3 The power spectrum from u (solid), v (dashed). a) the floats. b)the Eulerian field. c) high KE floats. d) low KE floats

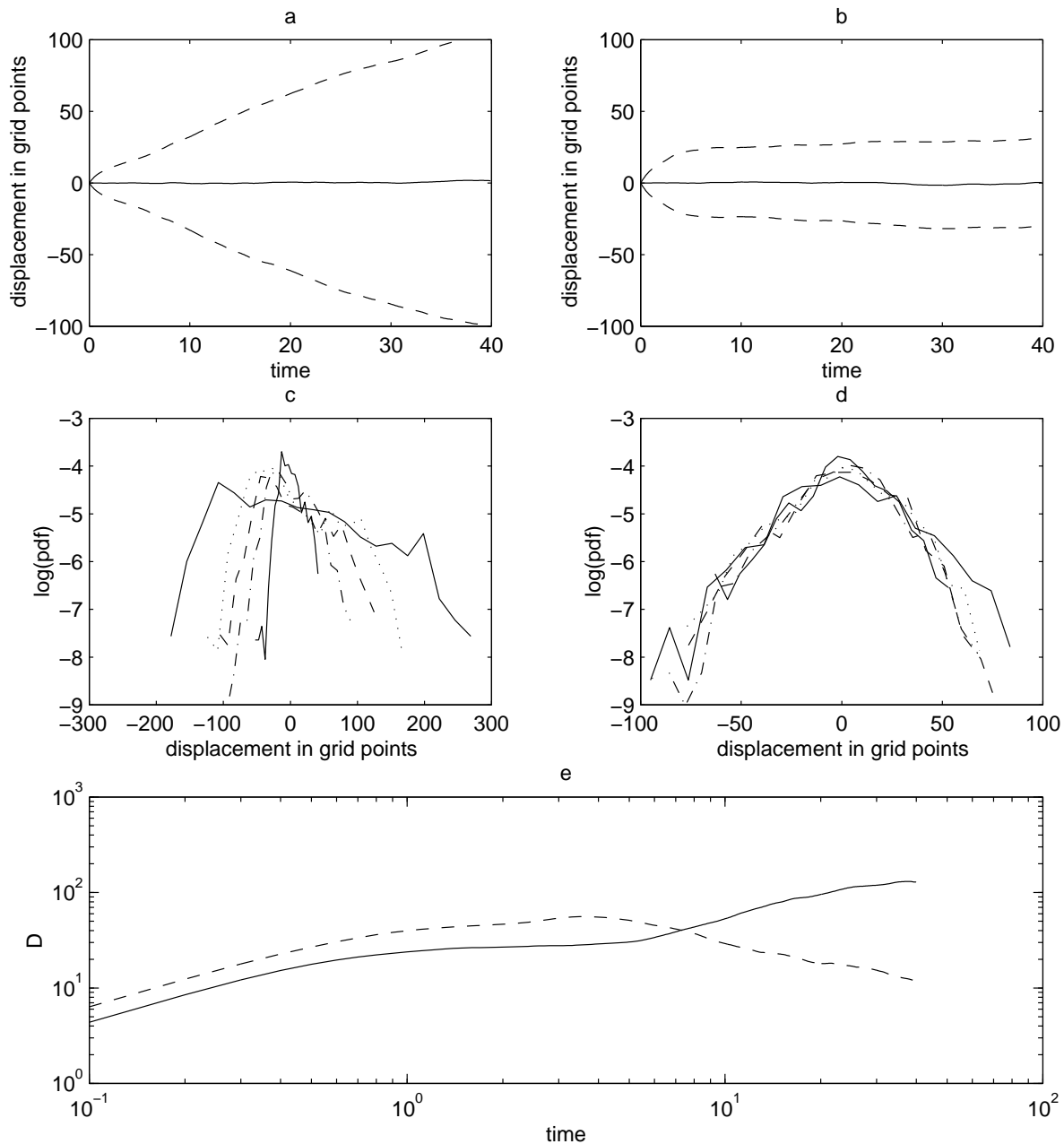


Figure 9: CASE 4 a) the solid line is the mean x-displacement, and the dashed are plus and minus A , the rms. b) the solid line is the mean y-displacement, and the dashed are plus and minus A , the rms. c) PDF of x displacement, inner solid is $t=5$, dashed dotted is $t=10$, dashed is $t=15$, dotted is $t=20$, outer solid is $t=40$. d) PDF of y displacement, the lines mean the same as for the x pdf. e) the dispersion coefficient, solid - in x, dashed - in y.)

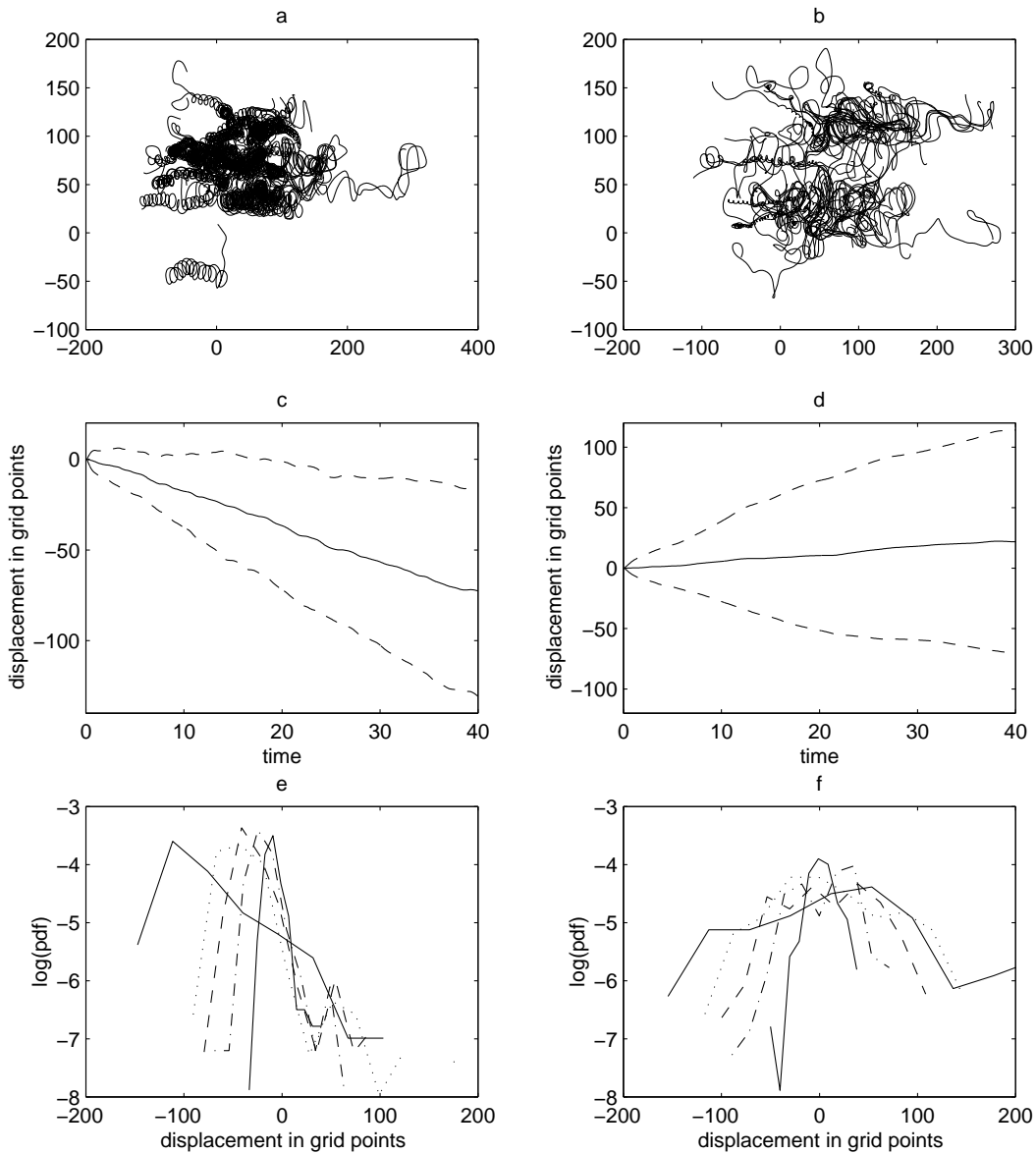


Figure 10: CASE 4 a) The trajectories of high KE floats. b) The trajectories of low KE floats. c) high KE floats: solid line is the mean x-displacement and the dashed lines are plus and minus Δ , the rms. d) low KE floats displacement same as c. e) high KE floats x PDF, inner solid is $t=5$, dashed dotted is $t=10$, dashed is $t=15$, dotted is $t=20$, outer solid is $t=40$. f) low KE floats x PDF, same as e.

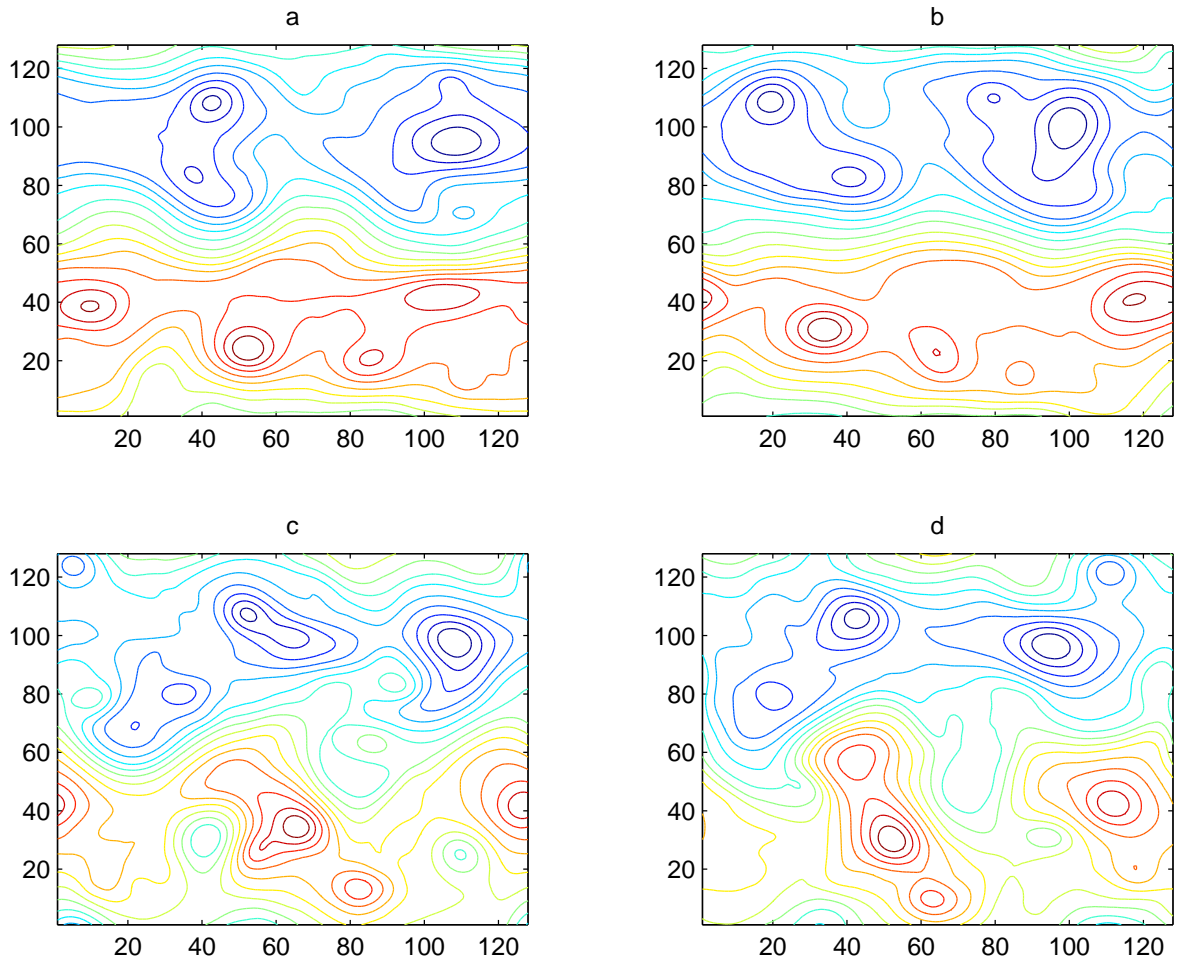


Figure 11: a,b) streamlines for KE ratio=1.4 at t=15,20. c,d) streamlines for KE ratio=.31 at t=15,20.

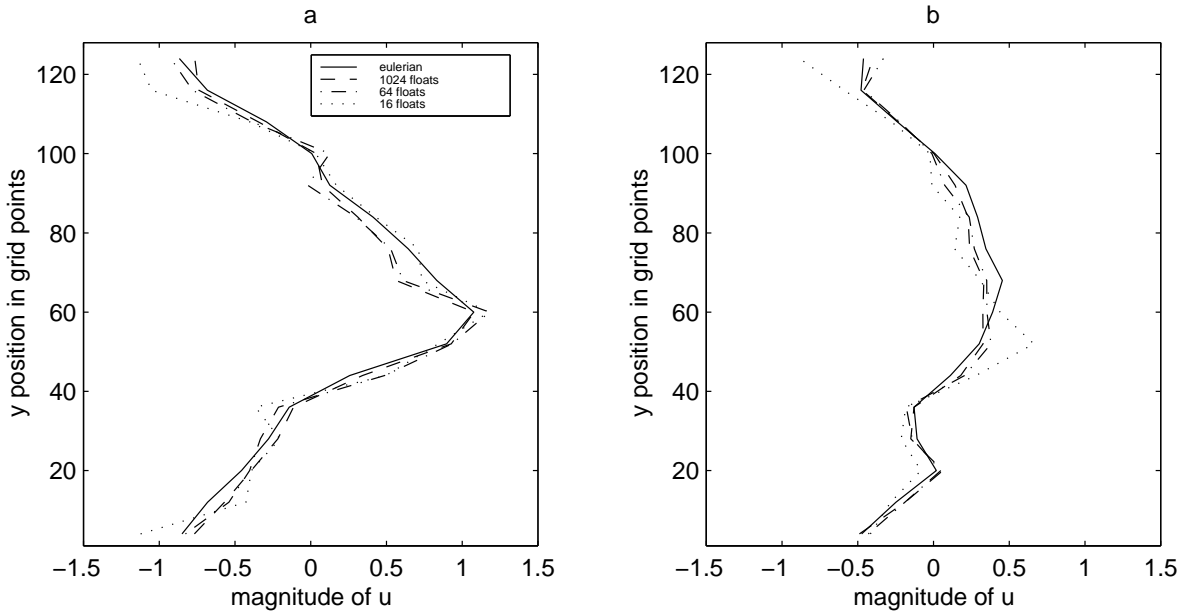


Figure 12: a) mean flow with KE ratio= 1.4 b) mean flow with KE ratio=.312

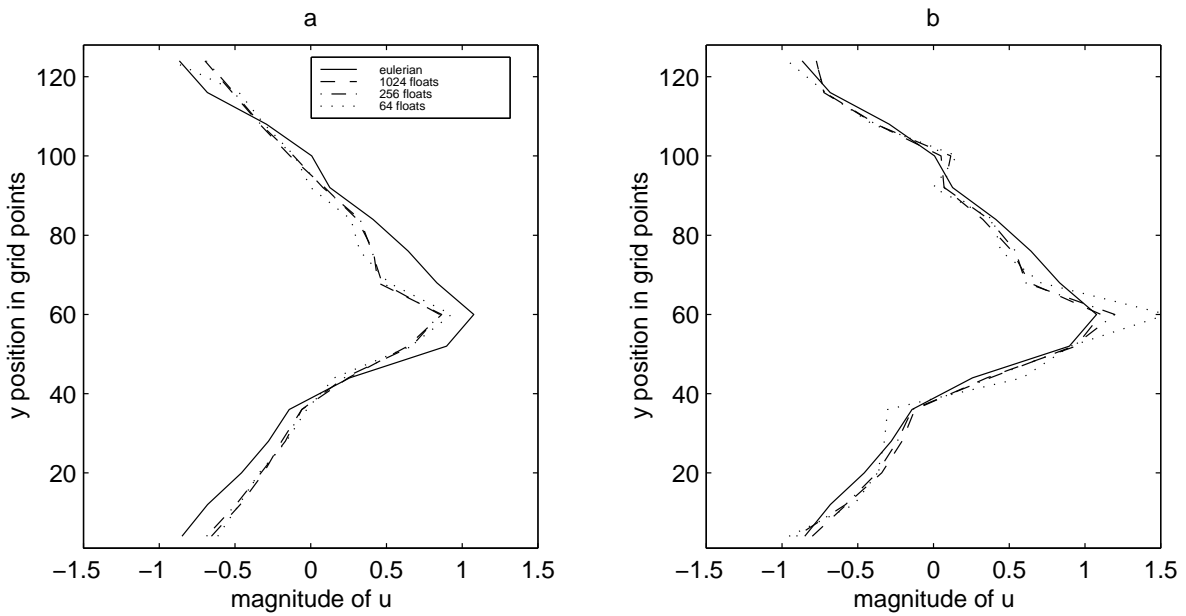


Figure 13: a) mean flow with KE ratio= 1.4 and u reconstructed from trajectories with $dt=2$
 b) mean flow with KE ratio=.14 with the velocity data thinned every $dt=2$

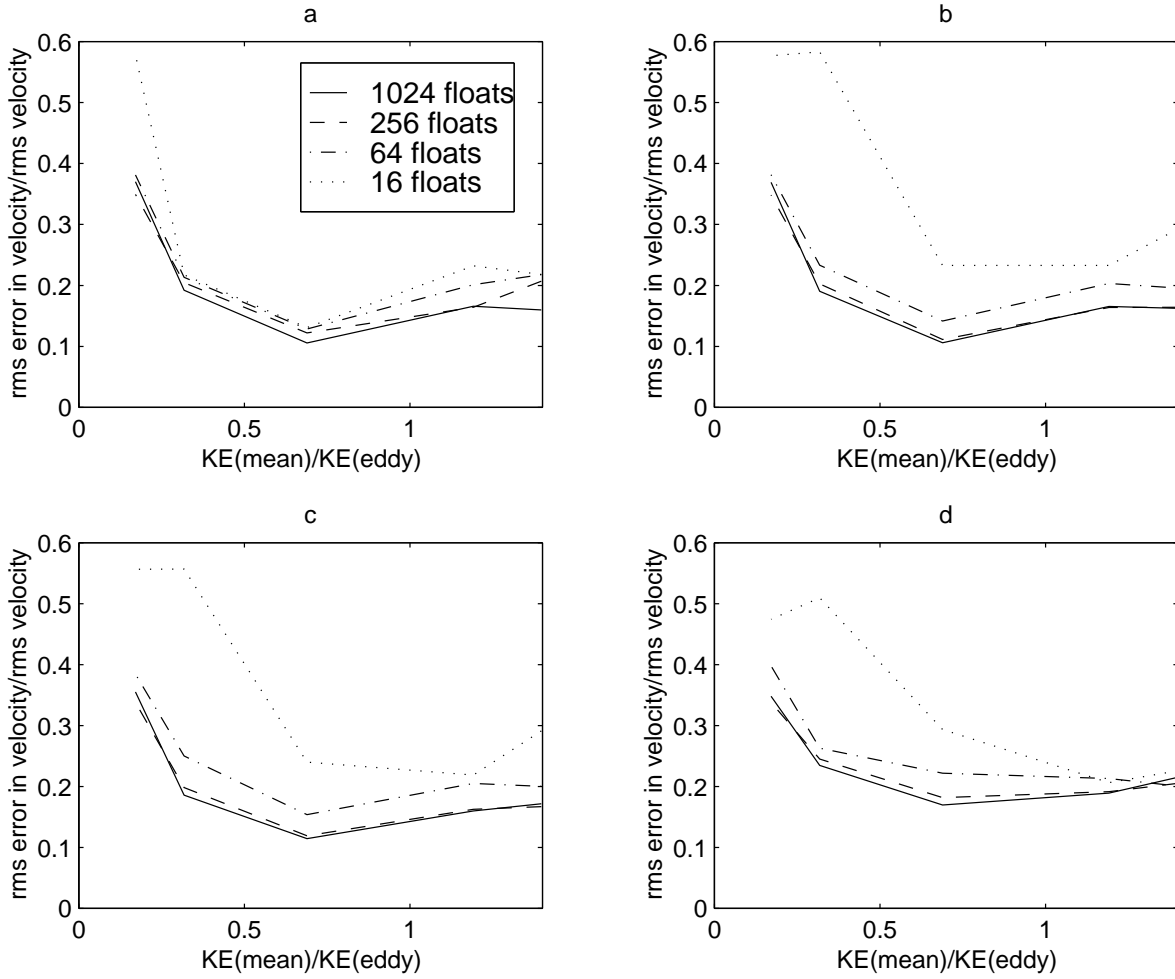


Figure 14: a) perfect data. b) reconstructed flow with $dt=.1$. c) reconstructed flow with $dt=.4$
d) reconstructed flow with $dt=1$